Temperature dependence of the Kohn anomaly in bcc Nb from first-principles self-consistent phonon calculations

Johan Tidholm,[1] Olle Hellman,[1] Nina Shulumba,[1] Sergei I. Simak,[1] Ferenc Tasnádi,[1] and Igor A. Abrikosov[1,2]
[1]*Department of Physics, Chemistry, and Biology (IFM), Linköping University, SE-581 83 Linköping, Sweden*
[2]*Materials Modeling and Development Laboratory, NUST "MISIS", 119049 Moscow, Russia*

(Received 18 July 2019; revised manuscript received 30 January 2020; accepted 6 February 2020; published 12 March 2020)

Using *ab initio* calculations, we have analyzed the influence of anharmonic effects on the electronic structure and the phonon-dispersion relations of body-centered-cubic (bcc) niobium (Nb) and investigated the temperature dependence of the Kohn anomaly in this metal. A comparison of the results obtained in the framework of the temperature-dependent effective potential method with those derived within the quasiharmonic approximation demonstrates the importance of the explicit treatment of the finite-temperature effects upon the theoretical description of bcc Nb lattice dynamics. In agreement with experimental results, the inclusion of anharmonic vibrations in our calculations leads to the disappearance of the Kohn anomaly for the acoustic mode in a vicinity of the Γ point with increasing temperature. Moreover, the calculated phonon self-energy indicates that the origin of the temperature dependence is related to the change of the electronic structure. We have calculated the temperature dependence of the electronic spectral function and analyzed the Fermi surface of Nb. A significant temperature-induced smearing of the electronic states has been identified as the origin of the disappearance of the Kohn anomaly in Nb at elevated temperature.

DOI: 10.1103/PhysRevB.101.115119

I. BACKGROUND

Body-centered-cubic (bcc) niobium (Nb) is a refractory metal with remarkable properties. It has a melting temperature of 2741 K and the highest superconductive critical temperature of all elements ($T_c = 9.25$ K) [1]. Consequently, the temperature dependence of the physical properties of Nb has attracted substantial interest. It is established that this metal shows unusual elastic and mechanical properties under pressure at low temperatures around T_c. Singh *et al.* [2] investigated Nb in a diamond anvil cell (DAC) using an x-ray beam perpendicular to the load axis and predicted an anomalous behavior of the compressive strength of Nb up to ∼12 GPa. Trivisonno *et al.* [3] measured the temperature dependence of the elastic constants of Nb in its normal metallic and superconducting states. Kawashima [4] reported an anomalous decrease of the elastic modulus, $C' = (C_{11} - C_{12})/2$, of the normally conducting state below T_c using a magnetic field higher than the critical field combined with ultrasonic measurements. Landa *et al.* [5,6] and Koči *et al.* [7] predicted a shear elastic softening of Nb from 20 to 150 GPa based on 0 K density functional theory (DFT) calculations. Based on the assumption that the thermal excitation of the electrons is the most significant temperature effect, Wang *et al.* [8] performed static DFT calculations, varying the electronic temperature and including the thermoelectronic entropy to predict the temperature dependence of the C_{44} shear elastic constant. The occurrence of the shear elastic softening has been suggested up to 2000 K. However, an absence of any phonon contribution which is expected to be significant at high temperatures calls for a reconsideration of this conclusion.

The phonon-dispersion relations of bcc Nb have been measured via inelastic neutron scattering [9–11] and also calculated in the framework of the density functional perturbation theory [12,13]. All report a "kink" in the vicinity of the Γ point in the phonon-dispersion relations at room temperature.

This peculiarity is believed to be a Kohn anomaly. Kohn showed [14] that the conduction electrons, i.e., the electrons at the Fermi energy, can interact with each other and phonons, causing singularities in the phonon-dispersion relations for metals under certain conditions. Specifically, electron-phonon coupling can occur if there is a phonon wave vector **q** that can connect two points on the Fermi surface. If the Fermi surface is composed of parallel flat sheets, the electron-phonon coupling for the wave vector **q** that connects the sheets—the nesting vector—diverges, resulting in a sharp kink in the phonon-dispersion relations at that specific wave vector **q**. In reality, no true divergences occur since the argument relies on a somewhat simplified picture, i.e., the predicted divergencies appear as smooth kinks.

The question this paper is addressing is the nature of the mechanism for the smoothing of the divergencies in the phonon-dispersion relations in bcc Nb. We are approaching the problem via lifting the assumption of well-defined,

temperature-independent electron and phonon quasiparticles. As the temperature is increased to 1030 K, the smoothing of the divergencies is so strong that they are no longer observable [15]. As temperature is increased, anharmonicity and electron-phonon coupling cause phonon bands to shift and broaden. Similarly, the thermal motion of ions breaks the perfect translational symmetry and ripple that the effective potential electrons feel, causing shifts and broadenings of the electronic states. In this paper, we show how finite-temperature effects can explain the disappearance of the Kohn anomaly with increased temperature as an almost purely geometrical effect originating in quasiparticle broadening.

II. METHODOLOGY

To estimate the finite-temperature electronic structure, we need to take the motion of ions into account and approximate the appropriate configuration average. The conventional quasiharmonic picture is inadequate for our goals since once the ions are in a thermally excited state the electron-phonon coupling will be different than for the static lattice, resulting in changed phonons. A self-consistent phonon procedure naturally deals with the interdependence of the electronic structure and phonons in a satisfactory manner [16,17]. Our self-consistent procedure is based on the temperature-dependent effective potential (TDEP) [18–20] approach, where a set of positions and forces is given as input and results in an effective harmonic (or higher-order) model,

$$H_{\mathrm{TDEP}} = U_0 + \sum_{i=1}^{N}\sum_{\alpha}^{\{x,y,z\}} \frac{\left(p_i^{\alpha}\right)^2}{2m_i} + \frac{1}{2}\sum_{\alpha,\beta}^{\{x,y,z\}}\sum_{i,j=1}^{N} \Phi_{ij}^{\alpha\beta} u_i^{\alpha} u_j^{\beta}. \tag{1}$$

U_0 in Eq. (1) is a temperature-dependent parameter that should be fitted in addition to the force constants. p_i^{α} and u_i^{α} denote the α component of momentum and displacement for ion i. m_i stands for the mass of the ith particle. $\Phi_{ij}^{\alpha\beta}$ is the second-order TDEP force constant matrix.

The positions that enter Eq. (1) need to sample a canonical ensemble. The Hamiltonian defined by the TDEP second-order force constant matrix provides the means to sample an ensemble from the effective phonons, and a self-consistent cycle can be constructed as described in the computational details below.

To enable us to evaluate the effect of including anharmonicity on phonon-phonon interactions, we calculate the phonon spectral function. Starting from the self-energy [21–23], $\Sigma_{\mathbf{q}s}(\Omega) = \Delta_{\mathbf{q}s}(\Omega) + i\Gamma_{\mathbf{q}s}(\Omega)$, where $\Delta_s^{\mathbf{q}}(\Omega)$ is the real part, $\Gamma_{\mathbf{q}s}(\Omega)$ is the imaginary part, and Ω gives the energy of the lattice excitation by $E = \hbar\Omega$ for mode $\omega_{\mathbf{q}s}$ at wave vector $\mathbf{q}$. The imaginary part of the self-energy can be calculated as [21–23]

$$\begin{aligned}\Gamma_{\mathbf{q}s}(\Omega) = \frac{\hbar\pi}{16}\sum_{\mathbf{q}'\mathbf{q}''s's''} &|\mathbf{\Phi}_{\mathbf{q}\mathbf{q}'\mathbf{q}''ss's''}|^2 \\ &\times\{(n_{\mathbf{q}'s'} + n_{\mathbf{q}''s''} + 1)\delta(\Omega - \omega_{\mathbf{q}'s'} - \omega_{\mathbf{q}''s''}) \\ &+ (n_{\mathbf{q}'s'} - n_{\mathbf{q}''s''})[\delta(\Omega - \omega_{\mathbf{q}'s'} + \omega_{\mathbf{q}''s''}) \\ &- \delta(\Omega + \omega_{\mathbf{q}'s'} - \omega_{\mathbf{q}''s''})]\},\end{aligned} \tag{2}$$

where $\mathbf{\Phi}_{\mathbf{q}\mathbf{q}'\mathbf{q}''ss's''}$ is derived from the third-order force constant matrix $\Phi_{ijk}^{\alpha\beta\gamma}$ as

$$\begin{aligned}\mathbf{\Phi}_{\mathbf{q}\mathbf{q}'\mathbf{q}''ss's''} = &\sum_{\alpha,\beta,\gamma}^{\{x,y,z\}}\sum_{i,j,k=1}^{N} \frac{\epsilon_{\mathbf{q}s}^{i\alpha}\epsilon_{\mathbf{q}'s'}^{j\beta}\epsilon_{\mathbf{q}''s''}^{k\gamma}}{\sqrt{\omega_{\mathbf{q}s}\omega_{\mathbf{q}'s'}\omega_{\mathbf{q}''s''}}} \\ &\times \frac{\Phi_{ijk}^{\alpha\beta\gamma}}{\sqrt{m_i m_j m_k}} e^{i(\mathbf{q}\cdot\mathbf{r}_i + \mathbf{q}'\cdot\mathbf{r}_j + \mathbf{q}''\cdot\mathbf{r}_k)}.\end{aligned} \tag{3}$$

Here, $\epsilon_{\mathbf{q}s}^{i\alpha}$ denotes the polarization vector of the mode $\omega_{\mathbf{q}s}$ at wave vector $\mathbf{q}$, and $\mathbf{r}_i$ is the equilibrium position for the ith ion. In Eq. (2), $n_{\mathbf{q}s}$ stands for the Bose-Einstein mean phonon occupation number at temperature T. The real part of the phonon self-energy is calculated from its imaginary part using the Kramers-Kronig transformation,

$$\Delta_{\mathbf{q}s}(\Omega) = \frac{1}{\pi}\mathcal{P}\int_{-\infty}^{\infty}\frac{\Gamma_{\mathbf{q}s}(\omega)}{\omega - \Omega}d\omega, \tag{4}$$

where $\mathcal{P}$ denotes the Cauchy principal value. From the self-energy, we obtain a spectrum,

$$S(\mathbf{q}, E) \propto \sum_{s}\frac{2\omega_{\mathbf{q}s}\Gamma_{\mathbf{q}s}(\Omega)}{\left[\Omega - \omega_{\mathbf{q}s}{}^2 - 2\omega_{\mathbf{q}s}\Delta_{\mathbf{q}s}(\Omega)\right]^2 + 4\omega_{\mathbf{q}s}^2\Gamma_{\mathbf{q}s}^2(\Omega)}, \tag{5}$$

for a phonon described by the wave vector $\mathbf{q}$ and its excitation energies E, which is what we call a phonon spectral function.

TDEP gives insight into the temperature dependence of the phonons. The configuration average that provides the effective phonons can also be used to determine the effective electronic structure. A complication is that we are using a supercell technique: the Brillouin zone in the configuration average is a significantly smaller and severely folded version of the bcc Brillouin zone. To translate the average over supercells to a single-particle effective band structure, we average the electronic band structure via unfolding [24–26],

$$\begin{aligned}P_{\mathbf{K}m}(\mathbf{k}) &= \sum_{n}|\langle\mathbf{K}m|\mathbf{k}n\rangle|^2 \\ &= \sum_{\mathbf{g}\in\mathrm{PCRL}}\left|C_{\mathbf{K}m}^{\mathrm{SC}}(\mathbf{g} + \mathbf{k} - \mathbf{K})\right|^2,\end{aligned} \tag{6}$$

$$A(\mathbf{k}, E) = \frac{1}{N_c}\sum_{c}\left\{\sum_{m}P_{\mathbf{K}m}^{c}(\mathbf{k})\delta\left(E_{\mathbf{K}m}^{c} - E\right)\right\}. \tag{7}$$

In Eq. (6), $P_{\mathbf{K}m}(\mathbf{k})$ is the spectral weight for a supercell Bloch state represented by the wave vector $\mathbf{K}$ and band index m at the primitive-cell wave vector $\mathbf{k}$. n is the band index for the primitive cell. The second equality is summed over the reciprocal lattice vectors $\mathbf{g}$ belonging to the primitive cell. $C_{\mathbf{K}m}^{\mathrm{SC}}$ is the coefficient of the supercell plane waves. By summing over all the supercell bands m with the energy $E_{\mathbf{K}m}$ equal to E for the wave vectors $\mathbf{K}$ that unfold to $\mathbf{k}$, a spectral function is obtained for the primitive-cell wave vector $\mathbf{k}$ and energy E, as the inner summation in Eq. (7). By summing over spectral weights for individual configurations and dividing by the number of configurations N_c, as the whole expression in Eq. (7), a configurationally averaged spectral function is acquired. In Eq. (7), $P_{\mathbf{K}m}^{c}$ is the spectral weight calculated as

in Eq. (6) and $E^c_{\mathbf{K}m}$ is the energy of band m at the wave vector $\mathbf{K}$ for the configuration c.

The above procedure projects the supercell states of a set of configurations onto the unit cell, defining a broadened spectra that we interpret as an electron spectral function.

As we are interested in the geometrical features of coupling of electrons and phonons at finite temperature, the temperature-dependent electronic and phononic spectral functions are the only ingredients we need to start discussing the temperature dependence of the Kohn anomaly. The unfolding procedure captures all orders of adiabatic electron-phonon coupling, but we must note that purely nonadiabatic terms are not included. At present, the exclusion of nonadiabatic terms seems to be an acceptable approximation for our needs.

III. COMPUTATIONAL DETAILS

We used a short *ab initio* molecular dynamics simulation (AIMD) as the initial seed for the self-consistent phonon calculations. Using TDEP, we calculated phonons from this initial seed. From these first "crude" phonons, we sampled the phase space in the following way [27,28]:

$$u_i^\alpha = \sum_{s=1}^{3N_a} \epsilon_s^\alpha A_{is} \sqrt{-2\ln\xi_1}\,\sin 2\pi\xi_2, \tag{8}$$

$$\dot{u}_i^\alpha = \sum_{s=1}^{3N_a} \omega_s \epsilon_s^\alpha A_{is} \sqrt{-2\ln\xi_1}\,\cos 2\pi\xi_2, \tag{9}$$

were u_i^α and $\dot{u}_i^\alpha$ are the Cartesian component in the α direction for the displacement from the thermal average and velocity for ion i. ξ_1 and ξ_2 are uniformly distributed variables with values between 0 and 1. ϵ_s^α stands for the Cartesian component of the polarization vector of the mode ω_s. The amplitude of these oscillations was set to be

$$A_{is} = \sqrt{\frac{2\hbar}{m_i\omega_s}\left(n_s + \frac{1}{2}\right)}, \tag{10}$$

which will include zero-point motion. n_s is the occupation number according to Bose-Einstein statistics and m_i is the mass of ion i. In practice, to "sample the phase space" means to populate supercells as microstates with the statistics according to a canonical ensemble given by the previously calculated phonons. Energies and forces were calculated by using density functional theory (DFT) for these populated supercells, which are what we previously have, and will continue to call configurations. We again use TDEP to calculate phonons and redo the phase-space sampling, obtaining a new set of configurations for which we again use DFT to calculate their energies and forces, which are sequentially used together with the displacement from the new set of configurations to calculate phonons using TDEP. For each iteration in the self-consistent phonon calculation, we used 30 configurations to guarantee convergence of the phonon-dispersion relations and phonon free energy; see the Appendix for more details regarding the convergence with respect to the number of configurations. After three iterations, the phonons showed no significant difference.

Materials expand with increasing temperature. To account for thermal expansion, we executed calculations on a volume-temperature grid. The volumes of the grid were equal to a $(6 \times 6 \times 6)$ supercell bcc structure of Nb with the lattice parameters 3.135, 3.238, 3,335, 3.427, and 3.513 Å. The temperatures were 0, 300, 1200, 2000, and 2700 K. The self-consistent procedure described above was used for each point on this grid. By interpolating the force constants on the volume-temperature grid, calculating Helmholtz free energy using TDEP and minimizing it for temperature, and including the extrapolation to 0 K, we obtained the volume as a function of temperature for zero pressure, which we will call the zero-pressure volume-temperature curve.

The calculations performed on the volume-temperature grid are not on the obtained volume-temperature curve. To obtain accurate phonon calculations on the volume-temperature curve, we additionally carried out the self-consistent phonon procedure on it. The lattice parameters for the volume-temperature curve were 3.323, 3.332, 3.357, 3.384, and 3.419 Å for the temperatures 0, 300, 1200, 2000, and 2700 K. As an initial seed, we used the phonons from the interpolated force constants. We only needed to perform one self-consistent phonon cycle with the same number of configurations previously used to obtain converged results. From the converged phonon calculations, the phase space was once again sampled. For each point on the curve, 10 new configurations were made for the phonon and electron spectral functions.

All the DFT simulations have been carried out with the projector augmented wave (PAW) method [29,30] implemented in the Vienna Ab initio Simulation Package (VASP) [31–34]. For the exchange-correlation energy functional, we applied the generalized gradient approximation (GGA) in the form suggested by Perdew, Burke, and Ernzerhof (PBE) [35]. The reciprocal space was probed according to a $(3 \times 3 \times 3)$ Γ-centered Monkhorst-Pack mesh [36]. We used a maximum energy of 600 eV for the plane-wave basis set. The electronic temperature was set to ∼1160 K if the temperature of the calculation did not exceed this value.

To unfold the electronic structure to what we will call electronic spectral functions, sometimes referred to as Bloch spectral functions, we took the thermal average of the 10 configurations on the volume-temperature curve. These were $(6 \times 6 \times 6)$ supercells with the reciprocal space sampled with a $(3 \times 3 \times 3)$ Γ-centered mesh, which means that we could unfold them to a unit cell with a $(18 \times 18 \times 18)$ k-point mesh. The unfolding has been performed using the BANDUP code [25,26]. For the actual plot, we interpolated the spectral function, band for band, on a finer mesh with 2400 points on the energy axis and 200 points between each high-symmetry point; the mesh was therefore of the size (2400×1000).

For the same 10 configurations, we calculated the phonon spectral function, perhaps better know as line shapes, $S(\mathbf{q}, E)$, or ideal inelastic neutron scattering. We used TDEP and a third-order Hamiltonian, obtaining the second- and third-order force constants, which we used to calculate the imaginary part of the self-energy [27]. The plot itself was calculated with a $(30 \times 30 \times 30)$ q-point mesh.

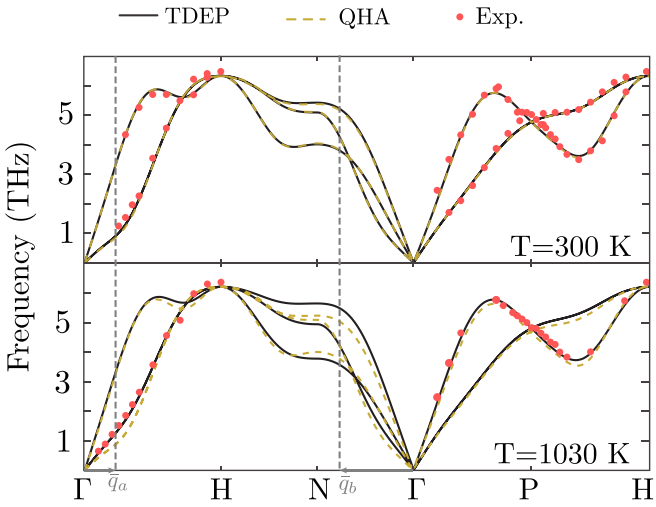

FIG. 1. Phonon-dispersion relations for bcc Nb at 300 and 1030 K. Solid lines show the results obtained using the second-order TDEP Hamiltonian. Dashed lines show the phonon frequencies derived by the quasiharmonic approximation (QHA). In the latter case, the temperature dependence of the phonon-dispersion relations is due to the temperature variation of the lattice parameter shown in Fig. 2. In the TDEP calculation, the force constants are temperature dependent, in addition to the lattice parameter. The dots show the experimental results from Refs. [9,15]. The vertical dashed lines shows the nesting vectors $\bar{q}_a$ and $\bar{q}_b$.

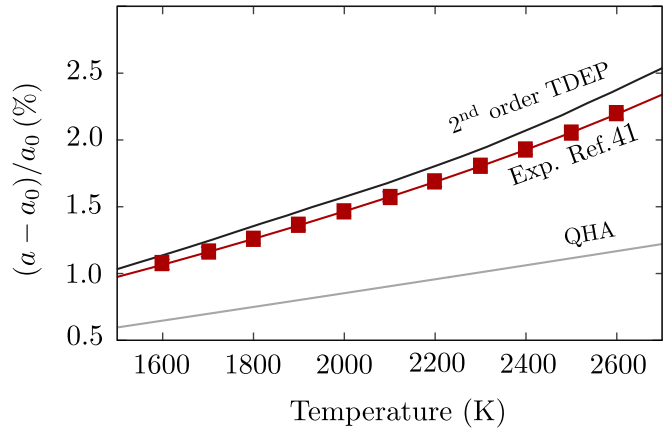

FIG. 2. Temperature dependence of lattice parameter $a(T)$ for bcc Nb between 1500 and 2700 K. It is expressed as a ratio $(a - a_0)/a_0$, where a_0 is the lattice parameter at 300 K. The experimental results are from Ref. [41], with the reference value of a_0 taken at $T = 293$ K. The calculated lattice parameter at $T = 0$ K was 3.32 Å. For both our TDEP and QHA calculations at $T = 300$ K, the reference value was 3.33 Å.

IV. RESULTS

Figure 1 shows the calculated phonon-dispersion relations at 300 and 1030 K in comparison with neutron-scattering experiments from Refs. [9,15]. The experimental results are shown with dots, while the dashed and solid lines display the result obtained by the quasiharmonic approximation (QHA) and with the second-order TDEP Hamiltonian, respectively. At room temperature (300 K), both theoretical approaches are in agreement with experiments. The phonon softening close to the Γ point is captured in our calculations. Not only the **q** vector, but also the size $(\Delta\omega/\omega)$ of the Kohn anomaly is reproduced well by both theories. As has been pointed out by Taylor [37], the size of the Kohn anomaly depends (i) on the strength of electron-phonon interaction and (ii) on the discontinuities occurring in the matrix elements of the interactions. Using an isotropic metal approximation, Taylor predicted the disappearance of the softening with increasing temperature [37]. The second-order TDEP results obtained at 1030 K and shown in Fig. 1 confirm this prediction, in agreement with experiment. On the contrary, the phonon softening within QHA is present even at a high temperature of 1030 K. An additional verification of our calculations can be seen in the calculated temperature dependence of the lattice parameter, which is presented in Fig. 2 and in good agreement with experiment, whereas the QHA underestimates the thermal expansion.

Phonon-phonon anharmonicity competes with electron-phonon coupling as the main mechanism for softening of phonons at finite temperature. To investigate the effects of pure anharmonicity, we calculated the phonon spectral function broadened from three-phonon processes, as presented in Figs. 3(a)–3(d). The central peaks of the spectral function closely track the second-order TDEP frequencies, while the phonon linewidths increase with temperature. Even close to the melting temperature at 2700 K, the spectral function is remarkably well defined, with clear quasiparticle peaks and no significant anharmonic shifts to speak of. This leads us to

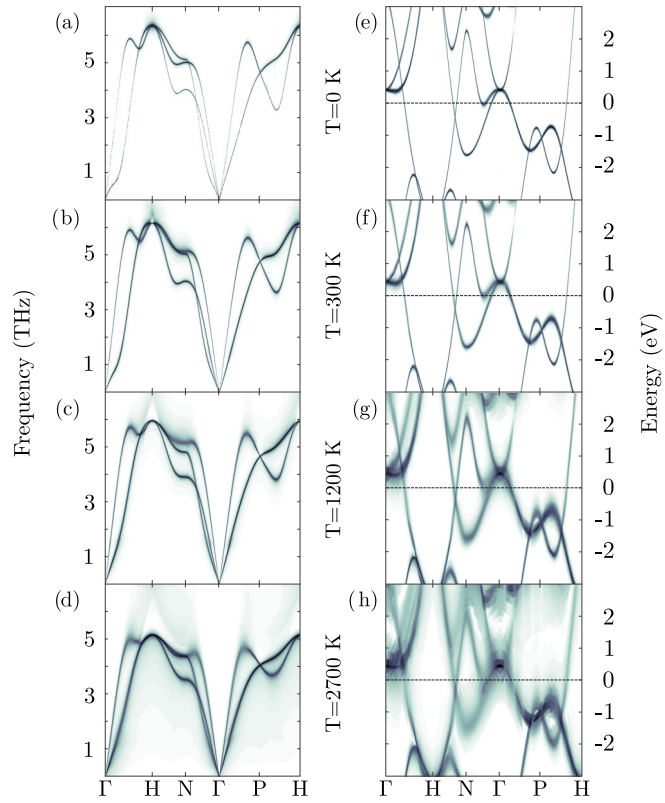

FIG. 3. (a)–(d) Phonon-dispersion relations calculated with the third-order TDEP Hamiltonian, including the finite linewidth, for bcc Nb in the temperature range 0 to 2700 K. (e)–(h) Electronic band structure of bcc Nb in the same temperature range.

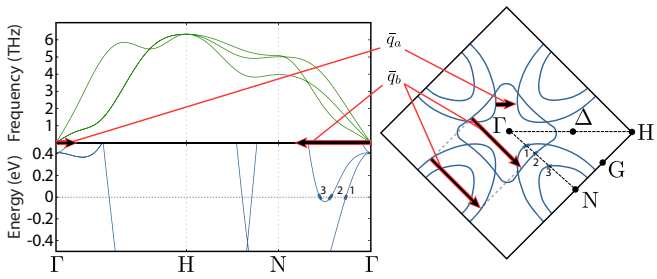

FIG. 4. Fermi surface of bcc Nb calculated at $T = 0$ K and the (100) plane cross sections. The nesting vectors $\bar{q}_a$ and $\bar{q}_b$ are marked out together with the parallel segments labeled 1, 2, and 3 on both the Fermi surface and the electron bands. We also see how the nesting vectors from the electronic structures correspond to the regional local softening in the 0 K phonon dispersions.

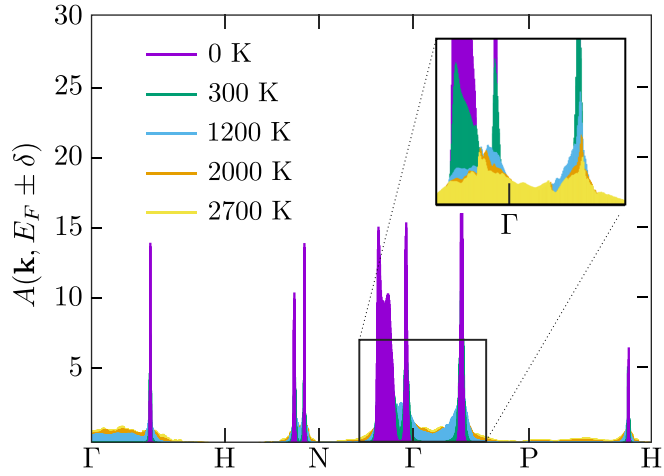

FIG. 5. Electron (or Bloch) spectral functions $A(\mathbf{k}, E)$ at different temperatures in the $[E_F - \delta, E_F + \delta]$ energy window around the Fermi energy (E_F) of Nb with $\delta = 1.7$ meV. The inset has an opposite order for temperature to expose the smearing of the peaks.

a conclusion that the main contributions to the temperature dependence of the phonons in Nb are electronic in origin.

The obtained electronic structure is shown in Figs. 3(e)–3(h). The amplified electron-phonon scattering with temperature leads to a decreased lifetime of the electrons, seen as the increasing linewidth of the bands in Figs. 3(e)–3(h). The line broadening, however, appears to be the dominant effect of the increasing temperature on the electronic structure, as the shape of the electronic bands appears to be unaffected.

It is well known that the Kohn anomaly in Nb is associated with certain *geometrical* features of its Fermi surface. Figure 4 shows the Fermi surface at $T = 0$ K and their (100) plane cross sections. The basic shape was calculated with the FERMISURFER software [38] and is in good agreement with previously published results [7,39]. The Fermi surface consists of three parts: two closed hole surfaces around the Γ and **N** points and a *jungle gym* tube. In Fig. 4, we have identified two nesting phonon wave vectors, $\bar{q}_a$ and $\bar{q}_b$. These vectors are also illustrated in Fig. 1, where one sees that it is at these points that the discrepancies between the QHA and fully temperature-dependent results are the largest.

This leads us to an interesting observation: the presence of parallel sheets in the Fermi surface should nominally lead to a divergence in the electron-phonon scattering at the specified **q** vectors, but no such divergence is observed in experiment or our calculations. We argue that the divergence is self-destroying in a sense: Fermi-surface nesting leads to large electron-phonon coupling. This broadens the electronic states, which in turn means that the Fermi surface becomes diffuse and not a sharp surface. With a diffuse Fermi surface, there will be no discrete nesting **q** vector, but a smooth distribution without any singular behavior. This idea is supported by our calculations of the finite-temperature electronic structure: even at 0 K, there is significant broadening of the bands in the vicinity of the Fermi energy, E_F, due to zero-point motion, for example, between $\Gamma - N$. The increased broadening of electronic bands with increasing temperature is closely tracked by the disappearance of the Kohn anomaly between $\Gamma - H$, and the temperature dependence of the phonon frequencies between $\Gamma - N$, as seen in Fig. 1.

To quantify this, we plot the electron spectral function integrated over a small energy range around E_F (± 1.7 meV) in Fig. 5. We are interested in the areas labeled 1 and 2 in Fig. 4; these areas are in the vicinity of the parallel segments of the Fermi surface for which the nesting vectors $\bar{q}_a$ and $\bar{q}_b$, marked out in Figs. 1 and 4, connect. If we look at Fig. 4, we see that the first peak in Fig. 5 when we go from Γ to N is related to the nesting vector $\bar{q}_a$, and the second peak in Fig. 5 between Γ and N is related to $\bar{q}_b$. With increasing temperatures, we observe in Fig. 5 that the two peaks related to the nesting vectors $\bar{q}_a$ and $\bar{q}_b$ are getting more smeared, and at 1200 K, they have became one diffuse blob with the neighboring peaks. Around this temperature, we observe in Figs. 1 and 3 that the "kink" between $\Gamma - H$ has disappeared and we observe a significant difference between the TDEP and the quasiharmonic phonon frequencies between $\Gamma - N$ in Fig. 1. This makes us argue that with increasing temperature, the electronic landscape is undergoing a transition of the topology of the Fermi surface, which should not be confused with Lifshitz electronic topological transition [40]. In our case, with increased temperature, we do not have a discrete sharp Fermi surface, but we have a diffused smeared one. However, if we would consider an *effective* Fermi surface, an isosurface fitted to the spectral function at the Fermi energy, its topology would, with increasing temperature, undergo a transition.

V. CONCLUSIONS

By using TDEP and fully including the anharmonic effects of lattice vibrations, we have studied temperature-dependent Kohn anomalies between $\Gamma - H$ and $\Gamma - N$ for the phonon frequencies in bcc Nb. The disappearance of these anomalies with increasing temperature becomes distinctly noticeable when compared with the quasiharmonic results at finite temperatures. From the low smearing and shift of the phonon spectral functions, we conclude that the phonon-phonon interactions are nearly negligible. What we, therefore, argue to majorly affect the phonons with increased temperature between $\Gamma - H$ and $\Gamma - N$ is the change in the electronic structure. We conclude that the electronic structure is changed by the smearing of the electronic states. This smearing affects

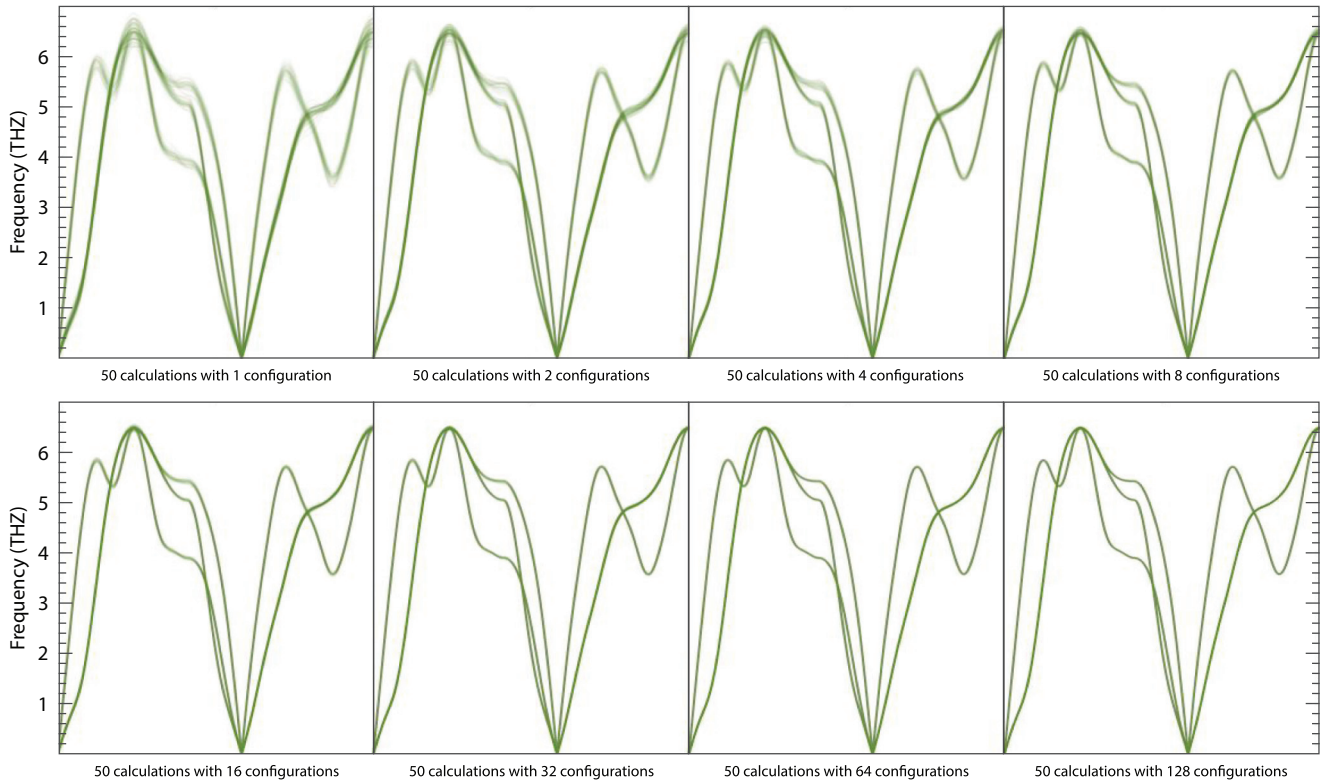

FIG. 6. Convergence of phonon-dispersion relations. From a pool of ∼1000, 50 calculations were performed with varying numbers of configurations. These numbers were 1, 2, 4, 8, 16, 32, 64, and 128. The broadening in this figure is a measure of the statistical error and should not be confused with the broadening, inverse phonon lifetime in Fig. 3.

the effective Fermi surface. We also observe that divergence in electron-phonon scattering is self-destroying, meaning that no sharp "kinks" will be observed in the phonon-dispersion relations for the nesting vectors. This is because the Fermi-surface nesting will make the Fermi surface diffuse and the nesting vector will no longer nest two parallel sharp segments, and therefore only smooth kinks will be observed.

ACKNOWLEDGMENTS

Support provided by the Swedish Research Council (VR) Projects No. 2015-04391 and No. 2019-05551, the Swedish Government Strategic Research Areas in Materials Science on Functional Materials at Linköping University (Faculty Grant SFO-Mat-LiU No. 2009-00971), Knut and Alice Wallenberg Foundation (Wallenberg Scholar Grant No. KAW-2018.0194), and Swedish Foundation for Strategic Research (SSF) Project No. EM16-0004 is gratefully acknowledged. Theoretical analysis of the electronic structure was supported by the Russian Science Foundation (Project No. 18-12-00492). The simulations were performed on resources provided by the Swedish National Infrastructure for Computing (SNIC) at the PDC Center for High Performance Computing at the KTH Royal Institute of Technology and at the National Supercomputer Centre at Linköping University.

APPENDIX: CONVERGENCE TEST

To test the convergence of the phonon dispersions with respect to the number of configurations used to extract the force constants, we used the following procedure: we generated a pool of ∼1000 configurations. From this pool, we select one configuration, and determine the force constants and the dispersion relations. Then we pick one new configuration and repeat the procedure about 50 times, which gives us a set of 50 phonon-dispersion relations. They are superimposed in the

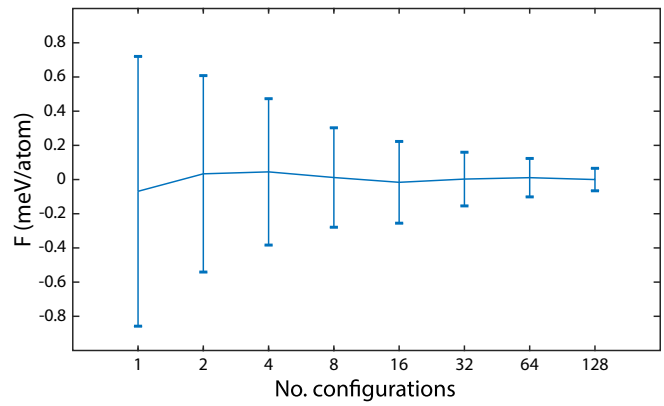

FIG. 7. Convergence of phonon free energies. The difference between the mean value and the mean value when 128 configurations were used is plotted. The error bars represent a confidence interval of 98%. From a pool of ∼1000, 50 calculations were performed with varying numbers of configurations. These numbers were 1, 2, 4, 8, 16, 32, 64, and 128.

first panel of the upper row in Fig. 6. The procedure is then repeated choosing 2, 4, 8, 16, 32, 64, and 128 configurations. At 16 random configurations, the statistical error is already of the order of the line thickness.

The specific dataset we used was generated at a lattice parameter of 3.335 Å and a temperature of 300 K, with the other calculational details equivalent to those in the main manuscript.

We can in a similar way determine the statistical error in the free energy, displayed in Fig. 7. Here we see that the 98% confidence interval is within 0.5 meV/atom at around 16 configurations.

[1] F. Cardarelli, *Materials Handbook: A Concise Desktop Reference* (Springer, London, 2008).

[2] A. K. Singh and H.-P. Liermann, J. Appl. Phys. **109**, 113539 (2011).

[3] J. Trivisonno, S. Vatanayon, M. Wilt, J. Washick, and R. Reifenberger, J. Low Temp. Phys. **12**, 153 (1973).

[4] K. Kawashima, Phys. Rev. B **76**, 212505 (2007).

[5] A. Landa, J. E. Klepeis, P. Söderlind, I. I. Naumov, O. Velikokhatnyi, L. Vitos, and A. Ruban, J. Phys.: Condens. Matter **18**, 5079 (2006).

[6] A. Landa, P. Söderlind, I. I. Naumov, J. E. Klepeis, and L. Vitos, Computation **6**, 29 (2018).

[7] L. Koči, Y. Ma, A. R. Oganov, P. Souvatzis, and R. Ahuja, Phys. Rev. B **77**, 214101 (2008).

[8] Y. X. Wang, H. Y. Geng, Q. Wu, X. R. Chen, and Y. Sun, J. Appl. Phys. **122**, 235903 (2017).

[9] B. M. Powell, P. Martel, and A. D. B. Woods, Phys. Rev. **171**, 727 (1968).

[10] Y. Nakagawa and A. D. B. Woods, Phys. Rev. Lett. **11**, 271 (1963).

[11] R. I. Sharp, J. Phys. C: Solid State Phys. **2**, 421 (1969).

[12] E. I. Isaev, S. I. Simak, I. A. Abrikosov, R. Ahuja, Y. K. Vekilov, M. I. Katsnelson, A. I. Lichtenstein, and B. Johansson, J. Appl. Phys. **101**, 123519 (2007).

[13] S. de Gironcoli, Phys. Rev. B **51**, 6773 (1995).

[14] W. Kohn, Phys. Rev. Lett. **2**, 393 (1959).

[15] B. M. Powell, A. D. B. Woods, and P. Martel, *Neutron Inelastic Scattering 1972: Proceedings of a Symposium, Grenoble, France, 1972* (International Atomic Agency, Vienna, Austria, 1972), pp. 43–52.

[16] M. L. Klein and G. K. Horton, J. Low Temp. Phys. **9**, 151 (1972).

[17] I. Errea, M. Calandra, and F. Mauri, Phys. Rev. B **89**, 064302 (2014).

[18] O. Hellman, I. A. Abrikosov, and S. I. Simak, Phys. Rev. B **84**, 180301(R) (2011).

[19] O. Hellman, P. Steneteg, I. A. Abrikosov, and S. I. Simak, Phys. Rev. B **87**, 104111 (2013).

[20] O. Hellman and I. A. Abrikosov, Phys. Rev. B **88**, 144301 (2013).

[21] A. A. Maradudin and P. A. Flinn, Ann. Phys. **15**, 337 (1961).

[22] A. A. Maradudin and A. E. Fein, Phys. Rev. **128**, 2589 (1962).

[23] R. A. Cowley, Adv. Phys. **12**, 421 (1963).

[24] V. Popescu and A. Zunger, Phys. Rev. B **85**, 085201 (2012).

[25] P. V. C. Medeiros, S. Stafström, and J. Björk, Phys. Rev. B **89**, 041407(R) (2014).

[26] P. V. C. Medeiros, Stepan S. Tsirkin, S. Stafström, and J. Björk, Phys. Rev. B **91**, 041116(R) (2015).

[27] N. Shulumba, O. Hellman, and A. J. Minnich, Phys. Rev. B **95**, 014302 (2017).

[28] N. Shulumba, O. Hellman, and A. J. Minnich, Phys. Rev. Lett. **119**, 185901 (2017).

[29] P. E. Blöchl, Phys. Rev. B **50**, 17953 (1994).

[30] G. Kresse and D. Joubert, Phys. Rev. B **59**, 1758 (1999).

[31] G. Kresse and J. Hafner, Phys. Rev. B **47**, 558 (1993).

[32] G. Kresse and J. Hafner, Phys. Rev. B **49**, 14251 (1994).

[33] G. Kresse and J. Furthmüller, Comput. Mater. Sci. **6**, 15 (1996).

[34] G. Kresse and J. Furthmüller, Phys. Rev. B **54**, 11169 (1996).

[35] J. P. Perdew, K. Burke, and M. Ernzerhof, Phys. Rev. Lett. **77**, 3865 (1996).

[36] H. J. Monkhorst and J. D. Pack, Phys. Rev. B **13**, 5188 (1976).

[37] P. L. Taylor, Phys. Rev. **131**, 1995 (1963).

[38] M. Kawamura, Comp. Phys. Commun. **239**, 197 (2019).

[39] A. R. Jani, N. E. Brener, and J. Callaway, Phys. Rev. B **38**, 9425 (1988).

[40] I. M. Lifshitz, Sov. Phys. JETP **11**, 1130 (1960).

[41] A. P. Miiller and A. Cezairliyan, Int. J. Thermophys. **9**, 195 (1988).